Spectroscopy on novel transition-metal compounds

Daisuke Takegami, Simone Altendorf, Chun-Fu Chang, Zhiwei Hu, and Liu Hao Tjeng[#]

Our goal is to understand how electron interactions in transition-metal compounds give rise to the extraordinary and often unexpected quantum phenomena observed in these systems. The complexity of their many-body electronic structure challenges us to develop approximations that capture the essential physics behind these phenomena. To address this, we are advancing cutting-edge x-ray spectroscopic techniques in conjunction with material-specific many-body model calculations.

In section 1.3 of the Status Report, we have already highlighted some of our key findings [1–3]: Through photon-energy-dependent photoemission and LDA+DMFT, we demonstrated that $CaCu_3Ru4O_{12}$ functions as an all-transition-metal Kondo system with an exceptionally high Kondo temperature [1]. By employing temperature-dependent HAXPES and full atomic multiplet cluster calculations, we inferred that paramagnetic $LaCoO_3$ is a highly inhomogeneous mixed-spin-state system exhibiting spin-state-specific local lattice relaxations. This finding offers an explanation for the long-debated temperature dependence of activation energies and the observed bad metal behavior [2]. Utilizing the orientation dependence of the HAXPES valence band spectra of the model compound ReO_3, we demonstrated the ability to obtain a direct image—without the need for calculations—of the active valence orbitals in crystalline materials. This innovative experimental method provides complementary information to ARPES and is applicable not only to bulk materials but also to thin films and multilayer systems [3].

We have further employed XAS and XMCD to determine the local charge, orbital, and spin states of transition metal ions in multi-component double and quadruple perovskites [4–7], aiming to elucidate their unusual magnetic and multiferroic properties. Similar studies, including HAXPES, have been conducted on compounds with more complex crystal structures and compositions [8–15].

In this website report, we highlight several intriguing and unexpected aspects uncovered during our investigations of Ba_2CoO_4 [16], Mg-doped Ti_2O_3 [17, 18], $FeWO_4$ [19, 20], and $LaCoO_3$ multilayers [21].

Electronic structure of the high-spin Co^{4+} system Ba_2CoO_4 [16]

High-oxidation state transition metal oxides represent a fascinating class of materials. In these systems, the O $2p$ to transition metal $3d$ charge transfer energy Δ is often expected to be negative, leading to a scenario where the O $2p$ band can cross the Fermi level, resulting in metallic p-type behavior. Notable examples include $SrCoO_3$ and Sr_2CoO_4, where the Co ions are octahedrally coordinated. Yet, $BaCoO_3$ is semiconducting, with its small band gap attributed to the face-sharing nature of the CoO_6 octahedra. This structural arrangement causes the O $2p$ ligand holes to exhibit poor inter-octahedra (CoO_6) hopping, a situation markedly different from $SrCoO_3$ and Sr_2CoO_4, which feature corner-sharing CoO_6 octahedra. Interestingly, the Co ions in $SrCoO_3$ and Sr_2CoO_4 are considered to adopt an intermediate spin (IS, $S = 3/2$) state, while in $BaCoO_3$, they exhibit a low spin (LS, $S = 1/2$) state.

Ba_2CoO_4 is another high-oxidation state compound, but it is composed of CoO_4 tetrahedra. The material is an antiferromagnetic semiconductor with a Néel temperature of approximately 25 K and large moments that suggest a $S = 5/2$ high-spin (HS) state for the Co ions. Our goal here is to investigate why this high-oxidation-state compound is not metallic and why it exhibits such large local moments.

We performed XAS measurements at the Co $L_{2,3}$ and O K edges and confirmed the formal 4+ valence of the Co ion using reference spectra. Through full atomic multiplet configuration interaction calculations, we determined that the crystal field parameter $10Dq$ that best reproduces the Ba_2CoO_4 spectrum is about -0.5 eV, confirming that the Co ions are indeed in the HS S=5/2 state. Interestingly, the calculations also revealed that for $10Dq$ more negative than about -2.0 eV, the Co would transition to the LS S=1/2 state. Since Ba_2CoO_4 is very far from this threshold, we can confidently conclude that the HS state in Ba_2CoO_4 is highly stable.

Our valence band photoemission spectrum is represented by the black curve in the top panel of Fig. 1. This spectrum cannot be adequatley explained by LDA band structure calculations, as shown by the grey curve in the bottom panel of Fig. 1. However, using the full atomic multiplet configuration interaction calculations, we successfully achieved a good simulation, as depicted by the green curve in the middle panel of Fig. 1. This result was obtained with a charge transfer energy Δ = -3.5 eV. A positive Δ would indicate that the lowest configuration is the Co $3d^5$ and that the Co $3d^6\underline{L}$ configuration is

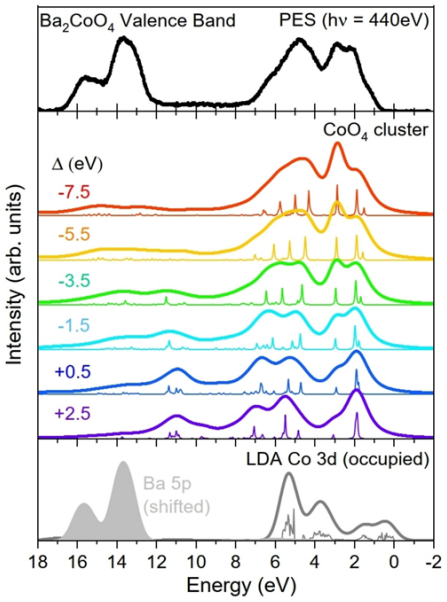

Fig. 1: Valence band photoemission of Ba_2CoO_4 taken at $h\nu$ = 440 eV photon energy (top panel) together with the Co 3d spectral weight from the CoO_4 cluster calculation for a range of charge transfer energy values Δ, from +2.5 to -7.5 eV (middle panel) and the LDA calculation in the antiferromagnetic state (bottom panel).

Δ higher in energy, and the Co $3d^7\underline{L}^2$ higher by $2\Delta+U$, and so on, where $\underline{L}$ denotes a hole in the O $2p$ ligand of the CoO_4 cluster. However, the negative value of Δ = -3.5 eV implies that the primary charge configuration of Co is not $3d^5$ (only 19% weight) but predominantly $3d^6\underline{L}$ (52%), followed by $3d^7\underline{L}^2$ (26%) with a small contribution from $3d^8\underline{L}^3$ (3%). This high oxidation state of the Co ions is thus characterized by a significant delocalization of holes onto the oxygen ligands. Despite this delocalization, the formal valence of the Co system remains 4+ (or rather IV), with the symmetry consistent with the HS $3d^5$ configuration.

The excellent agreement between the experimental spectra and the CoO_4 cluster calculations justifies a-posteriori, the use a single-site configuration interaction approach. However, this approach might be inadequate for metallic materials where substantial intersite or inter-cluster charge fluctuations are present. As noted earlier, a *p*-type metallic behavior could be anticipated in high-oxidation-state transition metal oxides, but this does not manifest in Ba_2CoO_4, suggesting that the ligand holes exhibit weak hopping due to the poor connectivity of the CoO_4 tetrahedra within the crystal structure.

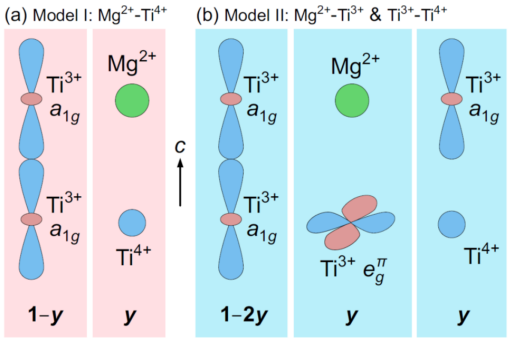

Fig. 2: (a) Model I, corresponding to a Ti^{3+}-Ti^{3+} pair with occupied a_{1g}-a_{1g} orbitals and Mg^{2+}-Ti^{4+} pair with empty Mg 3s and Ti 3d orbitals. Their relative populations are 1-y and y, respectively. (b) Model II, corresponding to a Ti^{3+}-Ti^{3+} pair with occupied a_{1g}-a_{1g} orbitals, Mg^{2+}-Ti^{3+} pair with empty Mg 3s and occupied Ti 3d e_g^{π} orbitals, and Ti^{3+}-Ti^{4+} pair with occupied Ti 3d a_{1g} and empty Ti 3d orbitals. Their relative populations are, 1-2y, y, and y, respectively.

Intra *c*-axis dimer hybridization and mixed valency in Mg-doped Ti_2O_3 [17,18]

Corundum-type Ti_2O_3 consists of Ti-Ti pairs within face-sharing TiO_6 octahedra. The Ti-Ti distance within these pairs gradually shortens as the temperature decreases from 600 to 400 K, during which Ti_2O_3 undergoes a metal-to-insulator transition. The reduction in Ti-Ti distance can be viewed as a dimerization or the formation of Ti^{3+}-Ti^{3+} molecular units. From a theoretical perspective, the Ti $3d$ a_{1g} states play a crucial role in forming the molecular orbitals that stabilize the insulating state.

It is interesting to study the effect of doping. Indeed, Mg substitution for Ti in the spinel-type $Mg_{1+x}Ti_{2-x}O_4$ system induces localized Ti spins and generates intriguing magnetic properties, suggesting that the Ti-Ti dimers are quickly disrupted. However, the situation for Ti_2O_3 may be quite different. In Ti_2O_3, the Ti-Ti pairs or dimers along the *c* axis in the face-sharing octahedra are structurally present at all temperatures. The interesting question is how the extra charge will be distributed over the lattice when Mg is substituted for Ti in the $Mg_yTi_{2-y}O_3$ system. Two possibilities can be envisioned. The first is that the Ti^{3+}-Ti^{3+} dimers remain intact, with the Mg^{2+} ion paired along the *c* axis with an isolated Ti^{4+} ion (see Model I in the left panel of Fig. 2). The second possibility is that the Ti-Ti dimers consist of Ti^{3+}-Ti^{4+} with the Mg^{2+} ion paired with an isolated Ti^{3+} ion (see Model II in the right panel of Fig. 2). Since the Ti-Ti distance along the *c* axis is shorter than those on the *ab* plane in Ti_2O_3, the first possibility benefits from the excitonic Madelung energy of Mg^{2+}-Ti^{4+} in-

side the face-sharing octahedra, as opposed to the Mg^{2+} and Ti^{4+} sites being farther apart.

We have investigated $Mg_yTi_{2-y}O_3$ (y = 0.01, 0.29, 0.63, 1.00) using HAXPES and polarization-dependent XAS at the Ti $L_{2,3}$ edges. We found that the initial substitution of Ti by Mg does not lead to the formation of Mg^{2+}-Ti^{4+} pairs (Model I), as previously thought. Instead, it creates Mg^{2+}-Ti^{3+} pairs, with the Ti^{4+} ions forming Ti^{3+}-Ti^{4+} pairs elsewhere in the structure. This conclusion was further supported by the observation that the holes introduced by the Mg substitution were found to be in the Ti-Ti pairs. We developed a model for the $y = 0.29$ composition, which consists of Mg^{2+}-Ti^{3+} pairs with e_g^π orbital symmetry, Ti^{3+}-Ti^{4+} pairs with a_{1g} orbital symmetry, and Ti^{3+}-Ti^{3+} pairs with a_{1g}-a_{1g} singlet bonds (Model II). This result highlights the crucial role of hybridization within the c-axis pairs not only in the Ti^{3+}-Ti^{3+} configuration, but especially in the Ti^{3+}-Ti^{4+} mixed valence state. This hybridization effect supersedes the Madelung gain energy associated with the Mg^{2+}-Ti^{4+} c-axis pair formation.

As the Mg content increased in the $y = 0.63$ composition, we observed a change in the orbital symmetry of the Ti^{3+} ions in the Ti^{3+}-Ti^{4+} pairs, with some converting from a_{1g} to e_g^π. The Ti-Ti bonds along the c axis tend to collapse at this hole-doping level, indicating a significant impact of hole doping on the electronic properties. These findings provide valuable insights into the electronic properties of transition-metal oxides and their metal-insulator transitions.

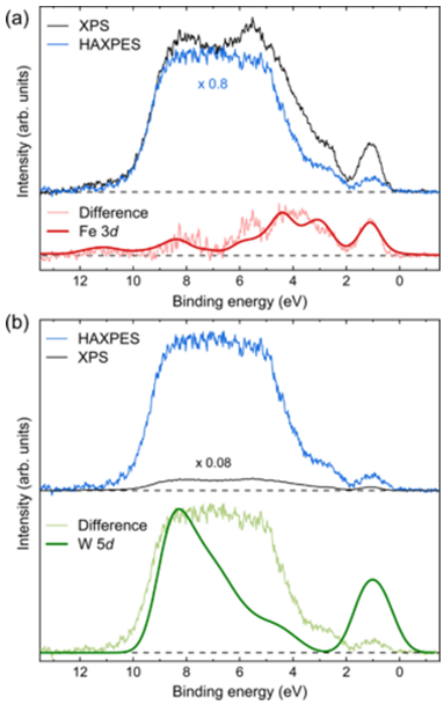

Fig. 3: Fe 3d and W 5d spectral weight deduced from the normalized and background-corrected valence band spectra taken at XPS and HAXPES photon energies. (a) Iron contribution: the HAXPES spectrum has been rescaled by a factor of 0.8 and the difference spectrum is compared to the results of the FeO_6 cluster calculation. (b) Tungsten contribution: the XPS spectrum has been rescaled by a factor of 0.08 and the difference spectrum is compared to the broadened W 5d density of states from the band structure calculation.

Electronic structure of the Fe^{2+} compound $FeWO_4$: correlations affecting the W 6*d* band [19, 20]

$FeWO_4$ is an antiferromagnetic semiconductor with a band gap of about 2 eV and a Néel temperature of 75 K. It belongs to the wolframite-type tungstates, which crystallize in a monoclinic structure where both iron and tungsten atoms are surrounded by six oxygen atoms. These octahedral FeO_6 and WO_6 clusters form two edge-shared zigzag chains along the [001] direction. The large electrochemical activity observed in this material has been attributed to reversible Fe^{2+}/Fe^{3+} surface redox reactions, making samples with large surface areas particularly attractive for applications. As a result, most reported studies have focused on various forms of nanocrystals, nanostructures, or polycrystalline materials. However, detailed studies of the electronic structure of monophase $FeWO_4$ single crystals are still lacking. Having recently developed a method for synthesizing millimeter-sized high-quality single crystals [19], we present here a comprehensive investigation of the electronic structure of $FeWO_4$, combining experimental photoelectron spectroscopy at different photon energies with theoretical analysis.

Figure 3 shows the valence band spectra measured at photon energies of 1486.6 eV (XPS) and 6.5 keV (HAXPES). These spectra exhibit a distinct peak near the Fermi level, at around 1 eV binding energy, which is well separated from a region of higher intensity between 2 and 10 eV. The two spectra are not identical due to the different photon energy dependence of the photoionization cross-sections of the Fe 3*d* and W 5*d* states. In fact, as explained in detail in Ref. [20], we can leverage this photon energy dependence to extract the separate contributions of the Fe 3*d* and W 5*d* shells to the valence band.

The bottom panel of Fig. 3a shows the extracted experimental Fe 3*d* spectral weight (light red curve) along with the result of a FeO_6 full multiplet configuration interaction cluster calculation (solid red curve). The overall agreement is satisfactory. The peak at 1 eV binding energy is a signature of the Fe^{2+} $3d^6$ high-spin configuration and can be assigned to the photoemission of the minority spin electron from the $3d^6$ initial state to a $3d^5$

$^6A_1$ final state. This is notably different from Fe^{3+} compounds with the $3d^5$ configuration, which do not exhibit a comparable feature near the Fermi level.

The bottom panel of Fig. 3b shows the extracted experimental W 5*d* spectral weight (light green curve) alongside the W 5*d* partial density of states (pDOS) from the band structure calculation (solid green curve). Significant deviations can be observed. The band structure calculation predicts a much larger intensity at 1 eV binding energy, which is related to the hybridization between tungsten and iron, but this intensity is overestimated in the calculation. On the other hand, the shape of the W 5*d* pDOS between 3 and 7 eV is significantly reduced compared to the experimental data, indicating that the contribution from tungsten is not adequately described by the band structure, and in this case, is significantly underestimated. A possible solution to this problem is provided by the FeO_6 cluster calculation, which shows that it is actually the iron that exhibits spectral features in this energy region. Consequently, the spectral weight from the 1 eV region is "transferred" to the 3-7 eV region due to hybridization with the iron, which contributes intensity there because of correlations not captured by the band structure model.

To conclude, the spectral weight of the Fe 3*d* states can be accurately described by the full multiplet configuration interaction calculation using an octahedral FeO_6 cluster. In contrast, the W 5*d* pDOS calculated from the band structure shows significant discrepancies. This is surprising at first, as electron correlation effects are not typically expected to play a prominent role for wide bands like the 5*d* states. However, the hybridization of the W 5*d* with the Fe 3*d* states, mediated by the O 2*p* orbitals, appears to be very strong. This strong hybridization highlights the necessity of using methods such as DFT + DMFT to capture these effects self-consistently.

Realization of high-spin and ferromagnetic $LaCoO_3$ monolayer [21]

Perovskite $LaCoO_3$ has been the subject of extensive and ongoing investigation due to the delicate competition between high-spin (HS) and low-spin (LS) states of Co^{3+} ions in octahedral coordination. Not surprisingly, it remains a significant challenge to deliberately tune the properties of $LaCoO_3$ for spintronic applications. For instance, it is still unclear how to stabilize ferromagnetism in $LaCoO_3$ thin films. In this study, our collaborators synthesized $SrIrO_3/LaCoO_3$ (SIO/LCO) superlattices on $SrTiO_3$ (STO), and together we investigated their magnetic properties using XAS and XMCD. The results are presented in Fig. 4. Panel (a) shows HAADF-STEM images of the SIO_5/LCO_1 (S_5/L_1) and SIO_1/LCO_1 (S_1/L_1) superlattices, demonstrating the high quality of the material. Panel (b) schematically summarizes the valence and spin states of the Co ions in the superlattices, as extracted from XAS data taken at the Co $L_{2,3}$ edges. Panel (c) displays a typical set of measured and calculated Co L_3 spectra, while panel (d) summarizes the fractions of HS Co^{3+}, LS Co^{3+}, and HS Co^{2+} in the different superlattice compositions.

It is surprising to observe that the fraction of HS Co^{3+} is significantly high in the superlattices, approximately 60%, which is much higher than the 25% found for bulk $LaCoO_3$ under ambient conditions [22]. Even more surprising is that the LS fraction of Co^{3+} decreases as the LCO layers become thinner, and it completely vanishes in the monolayer of LCO within the superlattice. Concurrently, the fraction of HS Co^{2+} increases, almost compensating for the decrease in LS Co^{3+} fraction. This suggests that charge transfer between Co^{3+} and Ir^{4+} to Co^{2+} and Ir^{5+} is energetically favorable. This is perhaps not surprising since it is even possible for Co^{3+} and Ir^{5+} to be converted to Co^{2+} and Ir^{6+}, as observed in Sr_2CoIrO_6 [23].

The presence of both HS Co^{3+} and HS Co^{2+} in equal quantities at the interface of SIO/LCO enables the double exchange mechanism, thereby stabilizing the metallic ferromagnetic state. This should be contrasted with the case of $La_{1.5}Sr_{0.5}CoO_4$, where equal quantities of LS Co^{3+} and HS Co^{2+} result in a highly insulating state due to the spin-blockade mechanism [24]. $La_{1.5}Sr_{0.5}CoO_4$ also exhibits a very low magnetic ordering temperature, primarily due to the non-magnetic character of LS Co^{3+}. In contrast, the ferromagnetic exchange interaction in the LCO monolayer is much stronger, as it has equal fractions of Co^{3+} and Co^{2+}, both in the HS state.

The observation that LS Co^{3+} is essentially absent in the monolayer LCO, with the HS Co^{3+} instead being stabilized, is a crucial aspect that requires further explanation. In previous studies, we investigated $Sr_2Co_{0.5}Ir_{0.5}O_4$ and found that all Co^{3+} ions were in the HS state [25]. This is a relatively rare case of HS Co^{3+} in octahedral coordination. However, in this material, the large Co-O distance of 1.97 Å corresponds very well with the HS Co^{3+} state. The key observation is that to stabilize Co^{3+} in the HS state, the Co-O coordination needs to have very large distances, specifically around 1.97–1.98 Å or larger. Merely providing "room", as in $La_{1.5}Sr_{0.5}CoO_4$, is insufficient, since in that case, the Co^{3+} forms strong covalent bonds with oxygen, resulting in shorter Co-O distances that stabilize the LS state. In the case of SIO/LCO, however, the inherent larger lattice of $SrIrO_3$ (SIO) exerts tensile strain on the $LaCoO_3$ (LCO) layer, stabilizing the HS

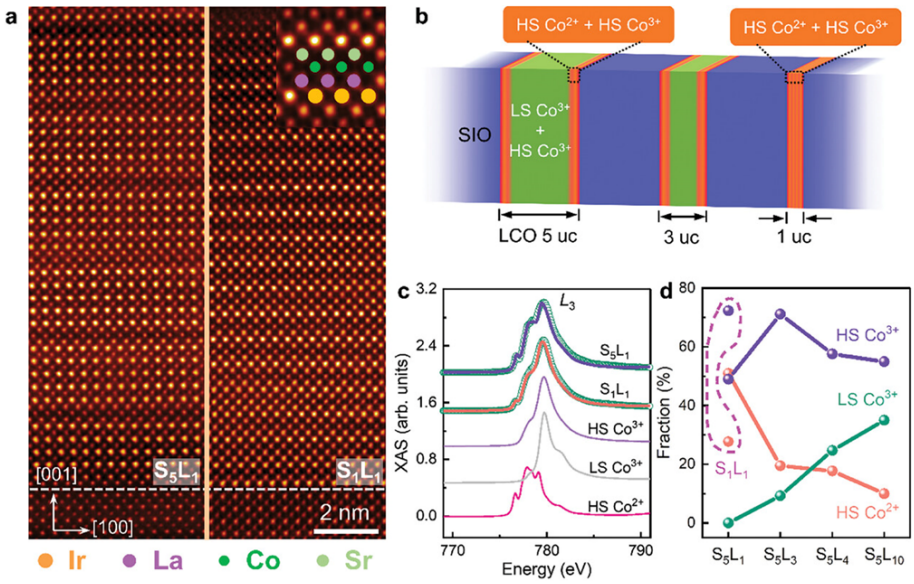

Fig. 4: $SrIrO_3/LaCoO_3$ (SIO/LCO) multilayers on $SrTiO_3$ (STO): a) HAADF-STEM images of SIO_5/LCO_1 (S_5/L_1) and SIO_1/LCO_1 (S_1/L_1); b) schematic valence state (2+/3+) and spin state (LS/HS, low-spin/high-spin) profile of the Co ions; c) Co L_3 XAS spectra and simulations; d) fractions of HS Co^{3+}, LS Co^{3+} and HS Co^{2+} in the different superlattice compositions.

state for Co^{3+}. This "clamping" effect is short-ranged for large lattice mismatches [26], which explains why LS Co^{3+} could appear if the LCO layer becomes thicker.

External Cooperation Partners

Antoine Maignan (CRISMAT, Caen , France); Jan Kuneš (Department of Condensed Matter Physics, Masaryk University, Brno, Czechia); Atsushi Hariki (Department of Physics and Electronics, Osaka Metropolitan University, Osaka, Japan); Arata Tanaka (Hiroshima University, Japan); Takashi Mizokawa (University of Tokyo, Japan); Youwen Long and Changqing Jin (Beijing National Laboratory for Condensed Matter Physics, Institute of Physics, Chinese Academy of Sciences, Beijing 100190, China); Zhaoliang Liao (National Synchrotron Radiation Laboratory, University of Science and Technology of China, Hefei, China); Robert J. Cava (Princeton University, United States).

References

[1]* *$CaCu_3Ru_4O_{12}$: A High-Kondo-Temperature Transition-Metal Oxide*, D. Takegami, C.-Y. Kuo, K. Kasebayashi, J.-G. Kim, C. F. Chang, C. E. Liu, C. N. Wu, D. Kasinathan, S. G. Altendorf, K. Hoefer, F. Meneghin, A. Marino, Y. F. Liao, K. D. Tsuei, C. T. Chen, K.-T. Ko, A. Günther, S. G. Ebbinghaus, J. W. Seo, D. H. Lee, G. Ryu, A. C. Komarek, S. Sugano, Y. Shimakawa, A. Tanaka, T. Mizokawa, J. Kuneš, L. H. Tjeng, and A. Hariki, *Phys. Rev. X* ***12*** *(2022) 011017*, https://dx.doi.org/10.1103/PhysRevX.12.011017

[2]* *Paramagnetic $LaCoO_3$: A Highly Inhomogeneous Mixed Spin-State System*, D. Takegami, A. Tanaka, S. Agrestini, Z. Hu, J. Weinen, M. Rotter, C. Schüßler-Langeheine, T. Willers, T. C. Koethe, T. Lorenz, Y. F. Liao, K. D. Tsuei, H.-J. Lin, C. T. Chen, and L. H. Tjeng, *Phys. Rev. X* ***13*** *(2023) 011037*, https://dx.doi.org/10.1103/PhysRevX.13.011037

[3]* *Direct imaging of valence orbitals using hard x-ray photoelectron spectroscopy*, D. Takegami, L. Nicolaï, Y. Utsumi, A. Meléndez-Sans, D. A. Balatsky, C.-A. Knight, C. Dalton, S.-L. Huang, C.-S. Chen, L. Zhao, A. C. Komarek, Y.-F. Liao, K.-D. Tsuei, J. Minár, and L. H. Tjeng, *Phys. Rev. Res.* ***4*** *(2022) 033108*, https://dx.doi.org/10.1103/PhysRevResearch.4.033108

[4]* *Magnetic and electric field dependent anisotropic magnetoelectric multiferroicity in $SmMn_3Cr_4O_{12}$*, G. Liu, Z. Liu, Y. Chai, L. Zhou, X. Shen, X. Ye, S. Qin, D. Lu, Z. Hu, L. H. Tjeng, H.-J. Lin, C.-T. Chen, X. Yu, and Y. Long, *Phys. Rev. B* ***104*** *(2021) 054407*, https://dx.doi.org/10.1103/PhysRevB.104.054407

[5]* *Comparative Study on the Magnetic and Transport Properties of B-Site Ordered and Disordered $CaCu_3Fe_2Os_2O_{12}$*, X. Wang, Z. Liu, H. Deng, S. Agrestini, K. Chen, J.-F. Lee, H.-J. Lin, C.-T. Chen, F. Choueikani, P. Ohresser, F. Wilhelm, A. Rogalev, L. H. Tjeng, Z. Hu, and Y. Long, *Inorganic Chemistry* ***61*** *(2022) 16929*, https://dx.doi.org/10.1021/acs.inorgchem.2c03030

[6]* *Realization of a Half Metal with a Record-High Curie Temperature in Perovskite Oxides*, Z. Liu, S. Zhang, X. Wang, X. Ye, S. Qin, X. Shen, D. Lu, J. Dai, Y. Cao, K. Chen, F. Radu, W.-B. Wu, C.-T. Chen, S. Francoual, J. R. L. Mardegan, O. Leupold, L. H. Tjeng,

Z. Hu, Y.-f. Yang, and Y. Long, *Adv. Mater.* ***34*** *(2022) 2200626*, https://dx.doi.org/https://doi.org/10.1002/adma.202200626

[7]* *Giant Exchange-Bias-Like Effect at Low Cooling Fields Induced by Pinned Magnetic Domains in Y_2NiIrO_6 Double Perovskite*, *Z. Deng, X. Wang, M. Wang, F. Shen, J. Zhang, Y. Chen, H. Feng, J. Xu, Y. Peng, W. Li, J. Zhao, X. Wang, M. Valvidares, S. Francoual, O. Leupold, Z. Hu, L. H. Tjeng, M. R. Li, M. Croft, Y. Zhang, E. Liu, L. He, F. Hu, J. Sun, M. Greenblatt, and C. Jin*, *Adv. Mater.* ***35*** *(2023) 085119e2209759*, https://dx.doi.org/10.1002/adma.202209759

[8]* *Magnetic Frustration in a Zeolite*, *D. Ni, Z. Hu, G. Cheng, X. Gui, W.-Z. Yu, C.-J. Jia, X. Wang, J. Herrero-Martín, N. Yao, L.-H. Tjeng, and R. J. Cava*, *Chemistry of Materials* ***33*** *(2021) 9725*, https://dx.doi.org/10.1021/acs.chemmater.1c03500

[9]* *Stability of the Pb divalent state in insulating and metallic $PbCrO_3$*, *J. Zhao, S.-C. Haw, X. Wang, L. Cao, H.-J. Lin, C.-T. Chen, C. J. Sahle, A. Tanaka, J.-M. Chen, C. Jin, Z. Hu, and L. H. Tjeng*, *Phys. Rev. B* ***107*** *(2023) 024107*, https://dx.doi.org/10.1103/PhysRevB.107.024107

[10]* *$Fe_2Co_2Nb_2O_9$: a magnetoelectric honeycomb antiferromagnet*, *A. Maignan, C. Martin, E. Tailleur, F. Damay, M. Mostovoy, X. Wang, Z. Hu, H.-J. Lin, C.-T. Chen, L. H. Tjeng, E. Suard, and F. Fauth*, *J. Mater. Chem. C* ***9*** *(2021) 14236*, https://dx.doi.org/10.1039/D1TC02950A

[11]* *$Fe_{4-x}Ni_xNb_2O_9$ ($x \leq 1$): Nickel impact on the magnetoelectric properties of $Fe_4Nb_2O_9$*, *A. Maignan, J.-N. Jiongo-Dongmo, C. Martin, O. Lebedev, F. Damay, X. Wang, C.-Y. Kuo, C.-F. Chang, Z. Hu, and L. H. Tjeng*, *Solid State Sciences* ***125*** *(2022) 106821*, https://dx.doi.org/https://doi.org/10.1016/j.solidstatesciences.2022.106821

[12]* *Electronic structure reconstruction by trimer formation in CsW_2O_6 studied by x-ray photoelectron spectroscopy*, *R. Nakamura, D. Takegami, A. Melendez-Sans, L. H. Tjeng, M. Okawa, T. Miyoshino, N. L. Saini, M. Kitamura, D. Shiga, H. Kumigashira, M. Yoshimura, K.-D. Tsuei, Y. Okamoto, and T. Mizokawa*, *Phys. Rev. B* ***106*** *(2022) 195104*, https://dx.doi.org/10.1103/PhysRevB.106.195104

[13]* *Interplay between strongly localized Eu 4f and weakly localized Nb 4d electrons in $Eu_3Nb_5O_{15}$*, *R. Nakamura, D. Takegami, A. Melendez-Sans, L. H. Tjeng, T. Miyoshino, K. Iwamoto, W. Sekino, M. Yoshimura, K.-D. Tsuei, T. Katsufuji, and T. Mizokawa*, *Phys. Rev. B* ***109*** *(2024) 165148*, https://dx.doi.org/10.1103/PhysRevB.109.165148

[14]* *Valence study of $Li(Ni_{0.5}Mn_{0.5})_{1-x}Co_xO_2$ and $LiNi_{1-x}Co_xO_2$: The role of charge transfer and charge disproportionation*, *D. Takegami, K. Kawai, M. Ferreira-Carvalho, S. Rößler, C.-E. Liu, C.-Y. Kuo, C.-F. Chang, A. Minamida, T. Miyazaki, M. Okubo, L. H. Tjeng, and T. Mizokawa*, *Phys. Rev. Mater.* ***8*** *(2024) 055401*, https://dx.doi.org/10.1103/PhysRevMaterials.8.055401

[15]* *High-pressure synthesis, crystal structure, and properties of iron-based spin-chain compound $Ba_9Fe_3Se_{15}$*, *J. Zhang, A. C. Komarek, M. Jin, X. Wang, Y. Jia, J. Zhao, W. Li, Z. Hu, W. Peng, X. Wang, L. H. Tjeng, Z. Deng, R. Yu, S. Feng, S. Zhang, M. Liu, Y.-f. Yang, H.-j. Lin, C.-T. Chen, X. Li, J. Zhu, and C. Jin*, *Phys. Rev. Mater.* ***5*** *(2021) 054606*, https://dx.doi.org/10.1103/PhysRevMaterials.5.054606

[16]* *Electronic structure of the high-spin Co^{4+} system Ba_2CoO_4*, *D. Takegami, Z. Hu, J. Falke, A. Meléndez-Sans, C.-E. Liu, C.-F. Chang, C.-Y. Kuo, C.-T. Chen, H. Guo, A. Komarek, A. Tanaka, S. Hébert, and L. H. Tjeng*, *Zeitschrift für anorganische und allgemeine Chemie* ***649*** *(2023) e202300077*, https://dx.doi.org/https://doi.org/10.1002/zaac.202300077

[17]* *Intra c-axis dimer hybridization and mixed valency in Mg-doped Ti_2O_3*, *T. Miyoshino, D. Takegami, A. Meléndez-Sans, R. Nakamura, M. Yoshimura, K.-D. Tsuei, K. Takasu, T. Okuda, L. H. Tjeng, and T. Mizokawa*, *Phys. Rev. B* ***107*** *(2023) 115145*, https://dx.doi.org/10.1103/PhysRevB.107.115145

[18]* *Linear dichroic x-ray absorption response of Ti-Ti dimers along the c axis in Ti_2O_3 upon Mg substitution*, *M. Okawa, D. Takegami, D. S. Christovam, M. Ferreira-Carvalho, C.-Y. Kuo, C. T. Chen, T. Miyoshino, K. Takasu, T. Okuda, C. F. Chang, L. H. Tjeng, and T. Mizokawa*, *Phys. Rev. B* ***108*** *(2023) 195108*, https://dx.doi.org/10.1103/PhysRevB.108.195108

[19]* *$FeWO_4$ Single Crystals: Structure, Oxidation States, and Magnetic and Transport Properties*, *A. Maignan, M. Schmidt, Y. Prots, O. I. Lebedev, R. Daou, C.-F. Chang, C.-Y. Kuo, Z. Hu, C.-T. Chen, S.-C. Weng, S. G. Altendorf, L.-H. Tjeng, and Y. Grin*, *Chemistry of Materials* ***34*** *(2022) 789*, https://dx.doi.org/10.1021/acs.chemmater.1c03640

[20]* *Electronic structure of the Fe^{2+} compound $FeWO_4$: A combined experimental and theoretical x-ray photoelectron spectroscopy study*, *S. G. Altendorf, D. Takegami, A. Meléndez-Sans, C. F. Chang, M. Yoshimura, K. D. Tsuei, A. Tanaka, M. Schmidt, and L. H. Tjeng*, *Phys. Rev. B* ***108*** *(2023) 085119*, https://dx.doi.org/10.1103/PhysRevB.108.085119

[21]* *Realization of Fully High-Spin State and Strong Ferromagnetism in $LaCoO_3$ Monolayer*, *J. Liu, L. Si, Q. Zhang, X. Wang, J. Freese, G. Harris, M. Wu, X. Zhang, T. Lin, R. Sutarto, J. Herrero-Martín, C. Guillemard, M. Valvidares, L. Li, X. Gao, Y. Ji, Z. Deng, Y. Hong, L. Wei, Y. Gan, L. Wang, G. Cheng, P. Gao, L. Gu, J. Zhang, Z. Hu, L. H. Tjeng, R. J. Green, K. Chen, and Z. Liao*, *Adv. Funct. Mater.* ***34*** *(2024) 2401859*, https://dx.doi.org/https://doi.org/10.1002/adfm.202401859

[22] *Spin State Transition in $LaCoO_3$ Studied Using Soft X-ray Absorption Spectroscopy and Magnetic Circular Dichroism*, *M. W. Haverkort, Z. Hu, J. C. Cezar, T. Burnus, H. Hartmann, M. Reuther, C. Zobel, T. Lorenz,*

A. Tanaka, N. B. Brookes, H. H. Hsieh, H.-J. Lin, C. T. Chen, and L. H. Tjeng, *Phys. Rev. Lett.* ***97*** *(2006) 176405*, *https://dx.doi.org/10.1103/PhysRevLett.97.176405*

[23] *Nature of the magnetism of iridium in the double perovskite* Sr_2CoIrO_6, *S. Agrestini, K. Chen, C.-Y. Kuo, L. Zhao, H.-J. Lin, C.-T. Chen, A. Rogalev, P. Ohresser, T.-S. Chan, S.-C. Weng, G. Auffermann, A. Völzke, A. C. Komarek, K. Yamaura, M. W. Haverkort, Z. Hu, and L. H. Tjeng*, *Phys. Rev. B* ***100*** *(2019) 014443*, *https://dx.doi.org/10.1103/PhysRevB.100.014443*

[24] *Spin Blockade, Orbital Occupation, and Charge Ordering in* $La_{1.5}Sr_{0.5}CoO_4$, *C. F. Chang, Z. Hu, H. Wu, T. Burnus, N. Hollmann, M. Benomar, T. Lorenz, A. Tanaka, H.-J. Lin, H. H. Hsieh, C. T. Chen, and L. H. Tjeng*, *Phys. Rev. Lett.* ***102*** *(2009) 116401*, *https://dx.doi.org/10.1103/PhysRevLett.102.116401*

[25] *Intricacies of the* Co^{3+} *spin state in* $Sr_2Co_{0.5}Ir_{0.5}O_4$*: An x-ray absorption and magnetic circular dichroism study*, *S. Agrestini, C.-Y. Kuo, D. Mikhailova, K. Chen, P. Ohresser, T. W. Pi, H. Guo, A. C. Komarek, A. Tanaka, Z. Hu, and L. H. Tjeng*, *Phys. Rev. B* ***95*** *(2017) 245131*, *https://dx.doi.org/10.1103/PhysRevB.95.245131*

[26] *Fe_3O_4 thin films: controlling and manipulating an elusive quantum material*, *X. Liu, C.-F. Chang, A. D. Rata, A. C. Komarek, and L. H. Tjeng*, *npj Quantum Materials* ***1*** *(2016) 16027*, *https://dx.doi.org/10.1038/npjquantmats.2016.27*

[#]hao.tjeng@cpfs.mpg.de